Exp Fluids (2007) 42:41–48
DOI 10.1007/s00348-006-0217-7

RESEARCH ARTICLE

Microscale Synthetic Schlieren

King-Yeung Yick · Roman Stocker · Thomas Peacock

Received: 26 May 2006 / Revised: 21 September 2006 / Accepted: 25 September 2006 / Published online: 1 November 2006

Abstract We develop the axisymmetric Synthetic Schlieren technique to study the wake of a microscale sphere settling through a density stratification. A video-microscope was used to magnify and image apparent displacements of a micron-sized random-dot pattern. Due to the nature of the wake, density gradient perturbations in the horizontal greatly exceed those in the vertical, requiring modification of previously developed axisymmetric techniques. We present results for 780 and 383 μm spheres, and describe the limiting role of noise in the system for a 157 μm sphere. This technique can be instrumental in understanding a range of ecological and environmental oceanic processes on the microscale.

K.-Y. Yick (✉)
Department of Mathematics,
Massachusetts Institute of Technology,
Cambridge, MA, USA
e-mail: kyyick@math.mit.edu

R. Stocker
Department of Civil and Environmental Engineering,
Massachusetts Institute of Technology,
Cambridge, MA, USA
e-mail: romans@mit.edu

T. Peacock
Department of Mechanical Engineering,
Massachusetts Institute of Technology,
Cambridge, MA, USA
e-mail: tomp@mit.edu

1 Introduction

Optical techniques based on the relation that typically exists between density and refractive index have long been used to visualize perturbations in a stratified fluid. Examples include the classic schlieren (Toepler 1864) and Moiré fringe techniques (Burton 1949). Synthetic Schlieren is a digital implementation of this idea that was recently developed for quantitative investigations of two-dimensional, linear internal-wave fields (Dalziel et al. 2000; Sutherland et al. 1999), and qualitative visualization of nonlinear internal waves (Peacock and Tabaei 2005). A similar digital technique, Background Oriented Schlieren, as reviewed by Venkatakrishnan and Meier (2004), has been applied to study the dynamics of compressible vortices (Richard and Raffel 2001). Most recently an axisymmetric formulation of Synthetic Schlieren has been developed (Onu et al. 2003) and used to study internal waves excited by a vertically oscillating sphere (Flynn et al. 2003). This approach exploits radial symmetry and inverse tomographic techniques to study axisymmetric perturbations in a stratified fluid.

To date, investigations using Synthetic Schlieren have been concerned with phenomena occurring on lengthscales in the range of 10 mm–1 m. However, many processes in stratified fluids occur at scales of microns to millimeters; in particular, ecologically and environmentally relevant phenomena in the ocean. Ubiquitous settling of marine snow aggregates (0.5–20 mm) and zooplankton fecal pellets (0.04–1 mm), for example, is responsible for a net export of limiting elements from the upper ocean, and can lead to strong accumulations of particles at density interfaces (McIntyre et al. 1995). The formation of these layers

could be favoured by the strong increase in drag associated with the stratification, predicted numerically (Torres et al. 2000). These layers in turn trigger accumulation of bacteria and phytoplankton, forming ecological hotspots of growth and productivity. Furthermore, there is indication that settling aggregates are themselves of major importance in channeling dissolved organic matter to the microbial loop via bacterial uptake, ultimately affecting the global carbon cycle (Azam and Long 2001). A full understanding of these processes requires the ability to visualize and understand the fluid mechanics of a stratified system at these small scales.

To study microscale particles settling in a homogenous fluid, it is convenient to scale up the size of an experiment, using a more viscous fluid to maintain dynamic similarity. This is not feasible in the presence of stratification, however, because one cannot appropriately scale diffusion of the stratifying agent. Therefore, the settling of microscale particles in a stratified ambient must indeed be studied on the microscale, demanding challenging experiments, of which there are few. One example is the study of Srdić-Mitrović et al. (1999) who tracked submillimeter spheres traversing sharp density interfaces.

To address our limited knowledge of processes involving small-scale disturbances in stratified fluids, we herein extend Synthetic Schlieren to submillimeter scales. In so doing, we operate on a scale two orders of magnitude smaller than any prior studies using this method. This presents practical challenges: smaller size particles require increasing magnification and generate ever weaker signals, which are eventually overwhelmed by noise. As a proof of concept, we use our experimental arrangement to study the flow structure in the wake of settling spheres, down to a diameter of 157 μm. Furthermore, for this process we find that perturbations of the horizontal density gradient far exceed those of the vertical, requiring modification of the axisymmetric method.

The layout of the paper is as follows. In Sect. 2 we describe the experimental set-up. Then, in Sect. 3, we present details of the axisymmetric Synthetic Schlieren method. The results of our test case study of a settling sphere are detailed in Sect. 4, prior to our conclusions in Sect. 5.

2 Experimental set-up

The experiments were performed in a 0.48 m high, 63 mm long and 25 mm wide perspex tank, with 5.4 mm thick walls, standing on a vibration-damped table, as shown in Fig. 1. The tank was filled with linearly stratified salt water using a double-bucket system (Oster 1965), and left to stand for several hours to allow dissipation of any residual flows. Several spherical density floats (American Density Floats) with densities covering the range 1,010–1,060 kg m^{-3} in intervals of 10.0 kg m^{-3} were then released into the tank to measure the vertical density gradient $d\rho/dz$. The small size of the floats (7 mm diameter) ensured that the density gradient was not distorted by their presence. Regular spacing of the vertical positions of the floats (i.e. their neutral buoyancy heights) confirmed the linearity of the density profile. The corresponding density gradient was determined from a linear fit to this data. There was no discernible motion of the floats, demonstrating the absence of any convection in the tank that could have affected the experimental results.

Experiments were performed using polystyrene spheres of diameter 3.16 mm and 750,383 and 157 μm, having density 1,050 kg m^{-3}. A 3-stage micro-manipulator mounted on top of the experimental tank facilitated the accurate deposition of the spheres, ensuring their release in the center of the tank and subsequent passing through the desired observation window as they settled. The micro-manipulator held a partially submerged conical injector (a 1 ml pipette) with an entrance diameter of 9.5 mm and an exit diameter of 3.3 mm, through which the spheres were released into the tank. The 3.16 mm and 780 μm spheres were deposited into the conical injector using a pair of tweezers. This was not feasible for the 383 and 157 μm spheres, which were instead mixed in very dilute quantities into a water sample, and then released into the conical injector using a 1 ml pipettor.

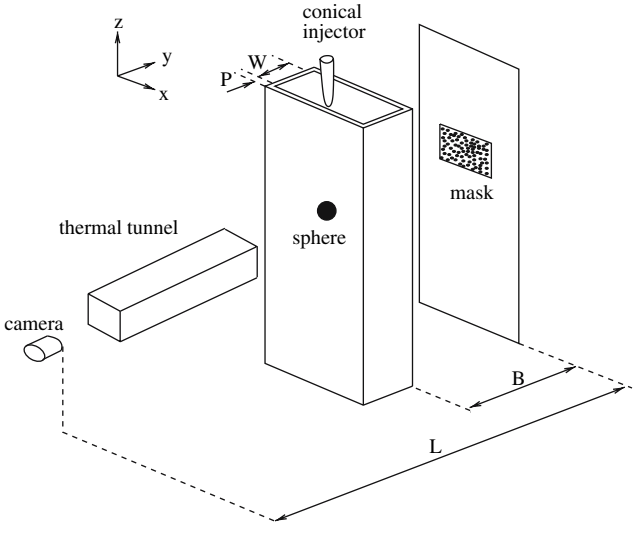

Fig. 1 Schematic of the experimental set-up

To image the wake of the settling spheres using Synthetic Schlieren, a 20 mm-square mask consisting of a random pattern of 35 μm dots was printed on transparency film using a high-resolution image-setter. The same mask was used for all experiments. The pattern was mounted a distance B = 83 mm behind the back wall of the tank, and imaged at 20 frames per second using a PCO 1600 CCD camera, operating at a resolution of 800×600 pixels. The camera was mounted on a Nikon SMZ 1000 stereo-microscope fitted with a P-Achro 0.5× objective, positioned a distance L = 189 mm in front of the mask, corresponding to the maximum working distance. Magnification factors of 7.5×, 10× and 15× were used, corresponding to observation windows of 15.2×11.4, 11.5×8.6, and 7.6×5.7 mm^2, respectively.

Images were captured using IPLab (Scanalytics) and the apparent displacements of the mask, caused by perturbations of the density stratification, were determined using DigiFlow (2006). To minimize the effect of thermal fluctations, a thermal isolation tunnel was placed between the microscope and the tank, and the reference image required by Synthetic Schlieren was an average of the first ten frames captured prior to the settling sphere entering the observation window.

3 Data analysis and processing

We begin by reviewing the axisymmetric Synthetic Schlieren technique detailed in Onu et al. (2003), before presenting the inverse tomographic method, with modifications relevant to studying the wake of a settling sphere.

3.1 Theoretical background

The path followed by a light ray in a stratified fluid satisfies Fermat's variational principle

$$\delta \int n(x,y,z)\mathrm{d}s = 0. \tag{1}$$

Here s is the along-the-light-ray coordinate and $n(x,y,z)$ is the refractive index field that is a function of across-tank (x), along-tank (y) and vertical coordinates (z) (see Fig. 1). Assuming the tangent to the light ray path always has a component in the y direction, the path can be described by $x(y)$ and $z(y)$: the former satisfies

$$\frac{\mathrm{d}^2x}{\mathrm{d}y^2} = \left[1 + \left(\frac{\mathrm{d}x}{\mathrm{d}y}\right)^2 + \left(\frac{\mathrm{d}z}{\mathrm{d}y}\right)^2\right]\frac{1}{n}\frac{\partial n}{\partial x}, \tag{2}$$

(Weyl 1954), and the latter the same equation with x and z interchanged. Provided that a light ray remains sufficiently parallel to the y direction, the nonlinear terms in (2) become negligible (for our set-up these are $O(10^{-2})$ or less), and the equations for $x(y)$ and $z(y)$ decouple. Since we anticipate horizontal density gradient perturbations, and thus horizontal refractive index gradient perturbations, to greatly exceed vertical ones (except perhaps in a small region in front of the sphere where isopycnals are compressed), our focus will be on the horizontal deflection of a light ray. By direct integration the x-component of a light-ray path is then

$$x(y) = x_i + y\cot\phi_i + \frac{1}{n_0}\int_0^y \int_0^{\hat{y}} \frac{\partial n}{\partial x}\mathrm{d}\hat{y}\,\mathrm{d}\hat{y}, \tag{3}$$

where x_i and ϕ_i are the location and angle of incidence in the horizontal plane at the point a light ray enters the tank, respectively.

Repeatedly applying Snell's law to a light ray that passes from a mask placed behind the tank to the camera, and making use of the relation $\frac{1}{n_0}\frac{\partial n}{\partial x} = \frac{\gamma g}{\rho_0}\frac{\partial \rho}{\partial x}$, the apparent horizontal displacement Δx of a feature in the mask due to a perturbation $\rho'(x, z)$ of the density field in a tank of width W is

$$\Delta x = -K_1 \int_0^W \frac{\partial \rho'}{\partial x}\mathrm{d}y - K_2 \int_0^W \int_0^y \frac{\partial \rho'}{\partial x}\mathrm{d}\hat{y}\,\mathrm{d}y. \tag{4}$$

Here $K_1 = \frac{\gamma g n_0}{\rho_0}\left(\frac{B}{n_a} + \frac{P}{n_p}\right)$, $K_2 = \frac{\gamma g}{\rho_0}$, P is the thickness of the container walls, n_a and n_p are the refractive indices of air and the tank walls, respectively, ρ_0 and n_0 are the characteristic density and refractive index of salt-water, g is the acceleration of gravity, and γ = 1.878 m^{-1} s^2 for salt-water.[1] For an axisymmetric disturbance extending over a characteristic length-scale V, the first term in Eq. 4 scales as BV (for $B >> P$), whereas the second term scales as V^2. For microscale applications, $V << B$ and the signal is dominated by the first integral.

In general, Eq. 4 is fully three-dimensional, but in the special case of an axisymmetric disturbance it can be solved using two-dimensional techniques. This was demonstrated for the axisymmetric wavefield gener-

[1] In deriving (4) we have corrected a sign in the presentation of the formulation in Dalziel et al. (2000), Flynn et al. (2003), Onu et al. (2003), and Sutherland et al. (1999); the results in those papers remain unaffected (S. Dalziel, personal communication, 2005/2006; B. Sutherland, personal communication, 2006). We have also included a multiplicative factor $1/n_0$ on the right-hand side of (4) that is missing in Flynn et al. (2003) and Onu et al. (2003).

ated by an oscillating sphere, where $\frac{\partial \rho'}{\partial z}$ was determined from apparent vertical displacements (Onu et al. 2003). Here we use a modified version of the same technique to measure $\frac{\partial \rho'}{\partial x}$, which itself is not axisymmetric, but can be derived from the axisymmetric quantity $\frac{\partial \rho'}{\partial r} = \frac{r \partial \rho'}{x \partial x}$. The integral equation we consider is therefore

$$\Delta x = -K_1 \int_0^W \frac{\partial \rho' x}{\partial r\, r} \mathrm{d}y - K_2 \int_0^W \int_0^y \frac{\partial \rho' x}{\partial r\, r} \mathrm{d}\hat{y}\, \mathrm{d}y. \tag{5}$$

This provides a means for determining $\frac{\partial \rho'}{\partial r}$ from measured apparent displacements Δx of a mask, as described in the following section.

3.2 Axisymmetric inverse tomography

First, we consider a $2V \times 2V$ horizontal cross-section of the wake behind a settling sphere, centered on the line of axisymmetry, and outside of which density perturbations are negligible. This domain is discretized into a series of rings in the manner shown in Fig. 2.

Consider the N-component vector of apparent horizontal displacements

$$\mathbf{D} = [\Delta x(x_1), \Delta x(x_2), \ldots, \Delta x(x_N)], \tag{6}$$

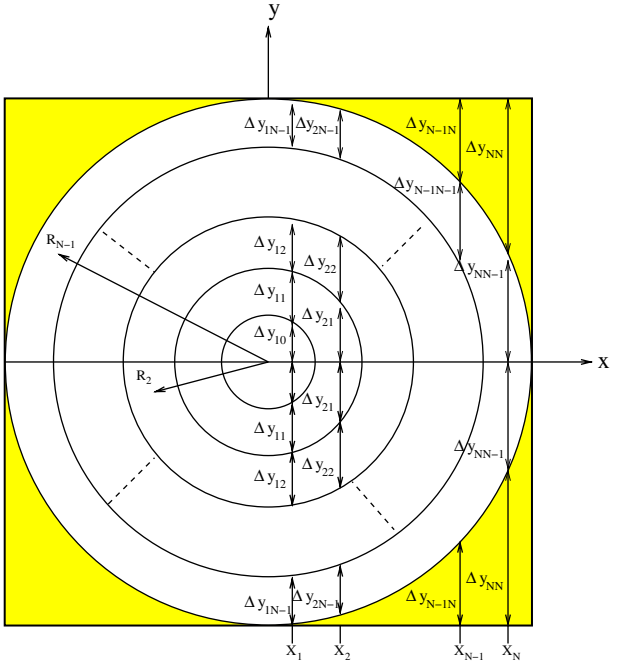

Fig. 2 Discretization of the horizontal plane used for tomographic inversion in the wake above the center of a settling sphere. The radial density gradient perturbation is constant within each ring and zero in the outer shaded region

in which x_i are the evenly spaced horizontal locations at which apparent displacements are measured. Since the wake structure is axisymmetric, $\frac{\partial \rho'}{\partial r}$ can be discretized as the N component vector

$$\mathbf{Q} = \left[\frac{\partial \rho'}{\partial r}(R_0), \frac{\partial \rho'}{\partial r}(R_1), \ldots, \frac{\partial \rho'}{\partial r}(R_{N-1})\right], \tag{7}$$

where R_i represents the mean of the inner and outer radii of the ith ring and we have assumed $\frac{\partial \rho'}{\partial r} = 0$ in the outermost (shaded) region in Fig. 2. Therefore, the two integrals in Eq. 5 can be approximated at x_i by

$$\int_{-V}^{V} \frac{\partial \rho'}{\partial r} \frac{x}{r} \mathrm{d}y \simeq 2 \sum_{j=i-1}^{N-1} \frac{\partial \rho'}{\partial r}(R_j) \frac{x_i}{R_j} \Delta y_{ij} = \mathbf{G_1 Q}, \tag{8}$$

and

$$\int_{-V}^{V} \int_{-V}^{y} \frac{\partial \rho' x}{\partial r\, r} \mathrm{d}\hat{y} \mathrm{d}y \simeq \sum_{k=1}^{2N} \Delta \tilde{y}_{ik} \sum_{j=1}^{k} \Delta \tilde{y}_{ij} \frac{\partial \rho'}{\partial r}(\tilde{R}_j) \frac{x_i}{\tilde{R}_j} = \mathbf{G_2 Q}, \tag{9}$$

where Δy_{ij} is the length of the horizontal transect in ring j (the central ring is labeled 0) corresponding to position x_i, as shown in Fig. 2; $\Delta \tilde{y}_{ij} = \Delta y_{i(j-N-1)}$ and $\tilde{R}_j = R_{j-N-1}$ if $j \geq N + i$, $\Delta \tilde{y}_{ij} = \Delta y_{i(N-j)}$ and $\tilde{R}_j = R_{N-j}$ if $j \leq N - i + 1$, and $\Delta \tilde{y}_{ij} = 0$ otherwise; and $\mathbf{G_1}$ and $\mathbf{G_2}$ are $N \times N$ mesh-dependent matrices.

The integral equation 5 is thus converted into the discrete problem

$$\mathbf{D} = -(K_1 \mathbf{G_1} + K_2 \mathbf{G_2}) \mathbf{Q}, \tag{10}$$

which can readily be solved by inverting the matrix $K_1\ \mathbf{G_1} + K_2\ \mathbf{G_2}$. Before analyzing the experimental data, we successfully tested the numerical implementation of this algorithm for the axisymmetric density perturbation $\rho' = e^{-r^2}$, for which Eq. 5 can be solved analytically.

4 Results and discussion

Our first application of the microscale Synthetic Schlieren technique was for a 780 μm diameter sphere settling in a stratification with $N = 1.31\ \mathrm{s}^{-1}$, and Reynolds number $Re = 4.1$. For these experiments we used 7.5 × magnification, corresponding to a resolution of 19 μm/pixel. Figure 3 shows an example of the wake behind the sphere, obtained by subtraction of the reference image. This technique is commonly referred to as qualitative Synthetic Schlieren (Dalziel et al. 2000),

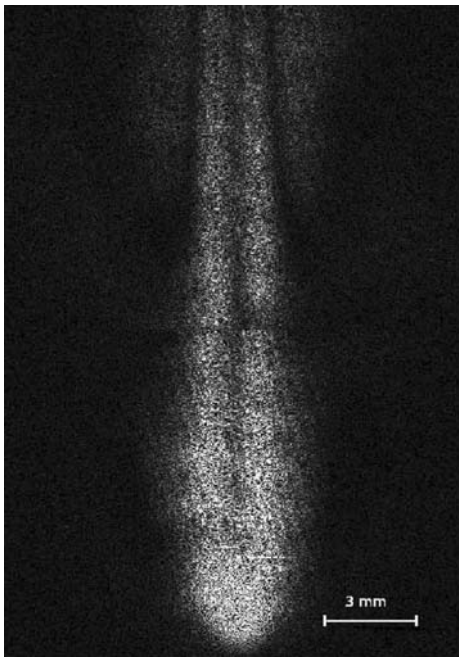

Fig. 3 Qualitative Synthetic Schlieren visualization at 7.5× of the wake of a 780 μm sphere. The figure is a composite of two frames. The intensity approximates the magnitude of the density gradient

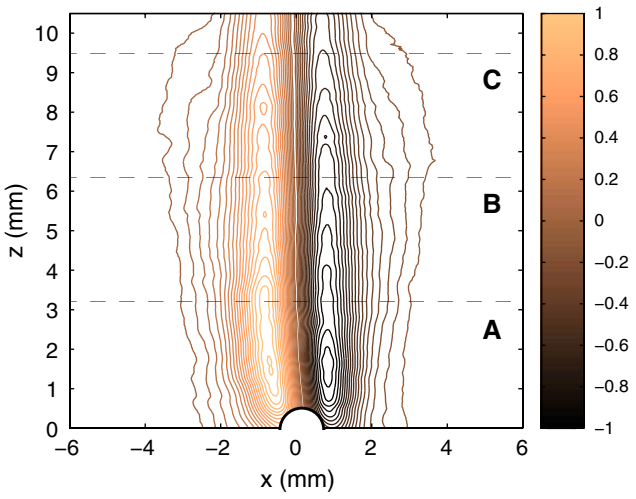

Fig. 4 Contours of the apparent horizontal pixel displacements Δx in the wake of a 780 μm sphere. The particle Reynolds number is Re = 4.1. The portion of the sphere in the field of view has been superimposed. Data along the three horizontal transects A, B, and C are presented in Figs. 5 and 6

and approximates the magnitude of the density gradient perturbations. Despite this relatively crude processing, the structure of the wake is already evident. It is highly symmetric about the dark vertical centerline, where distortions of the pattern are small. Furthermore, the wake is approximately 5-mm wide and more than 22-mm long, greatly exceeding the size of the sphere.

The structure of the wake, in particular its symmetry, is even more evident in Fig. 4, which presents a contour plot of the apparent horizontal displacements Δx of the mask. This data was obtained using the pattern-matching algorithms of DigiFlow (2006), with an interrogation-window of 19 pixels and a window-spacing of 16 pixels, corresponding to approximately 20 data points across the width of the wake. A spatial zero-phase, low-pass Butterworth filter was used to remove high-frequency noise prior to axisymmetric processing. Characteristic horizontal displacements were on the order of 0.5 pixels (9.5 μm), demonstrating good operating conditions for the pattern matching techniques, which are accurate to better than 0.1 pixels (Dalziel et al. 2000).

One practical difficulty of Synthetic Schlieren at the microscale is that the small depth of focus of the video-microscope requires the sphere to be very close to the mask (small B) in order to have both in focus. This conflicts with the demand that the sphere be sufficiently far from the mask to generate a strong enough signal, as discussed earlier in regards to Eq. 4, effectively precluding focusing on both the mask and the sphere at the same time. Thus the sphere itself cannot be clearly resolved in the image. While one could envisage an experimental set-up that includes a second, synchronized video-microscope focused on the sphere and capable of simultaneously tracking its location, we could visually determine the position of the sphere in each raw image to within one sphere radius. For the data in Fig. 4, the center of the sphere was approximately (x, z)=(0.3, –0.1) mm.

The apparent horizontal displacements Δx measured along a cross-section of the wake approximately four diameters above the sphere, indicated by the dashed line A in Fig. 4, are presented in Fig. 5. The horizontal density gradient perturbation $\frac{\partial \rho'}{\partial r}$ was then obtained from Δx using the axisymmetric algorithm detailed in Sect. 3. Figure 5 shows that the magnitude of $\frac{\partial \rho'}{\partial r}$ (~220 kg m^{-4}) is greater than the background vertical stratification (~180 kg m^{-4}), implying strong distortions of isopycnals by the settling sphere. In contrast to previous studies of internal waves, it is interesting to recognize that Synthetic Schlieren can reliably detect such dramatic nonlinear distortions of the background stratification. This is due to the region of influence of the sphere being highly localized and therefore still generating only a weak deflection of the light ray passing though the tank. In obtaining $\frac{\partial \rho'}{\partial r}$, we enforced $\Delta x = 0$ at either end of the profile, smoothly tapering it

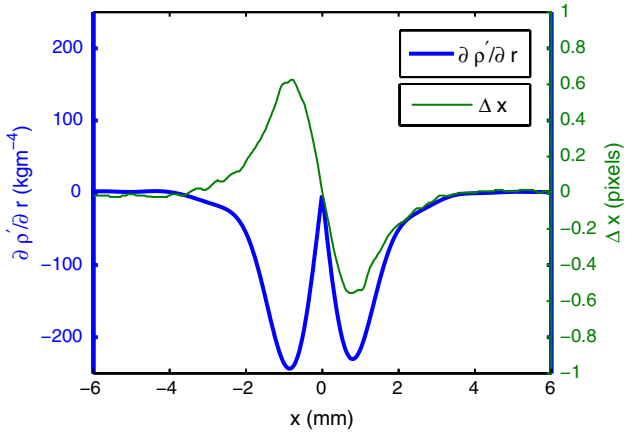

Fig. 5 Apparent horizontal displacements of the mask (*thin line*) and radial density gradient perturbation (*thick line*) for a 780 μm sphere measured along transect A in Fig. 4

off over the last 10 pixels. This was done to avoid far-field apparent displacements Δx, which are on the order of the background noise level (0.02 pixels), being amplified by the axisymmetric processing and deteriorating the density perturbation profile.

Integrating $\frac{\partial \rho'}{\partial r}$ along a radial transect and adding the background stratification yields the perturbed density ρ at a given cross-section of the wake. This is illustrated in Fig. 6 for the transects A, B, and C, indicated in Fig. 4, which are 4, 8, and 12 diameters above the sphere, respectively. The accuracy of the method is supported by the fact that, after integration across the wake, only a minor density mismatch exists between the far field on the left and the right of the sphere (<0.016 kg m^{-3}). As one might expect, Fig. 6 shows that lighter fluid is dragged downwards by the settling sphere. The fluid at the center of the wake has been dragged down a distance $\rho'/\frac{\partial \rho}{\partial z}$, corresponding to 1.9 mm for transect A, 1.6 mm for transect B, and 1.2 mm for transect C. We note that this corresponds to about 1 sphere diameter. The three transects show that the density perturbations diminish along the wake, although Fig. 4 reveals that there is a 2 mm region immediately behind the sphere in which the opposite is true.

To test the operational limits of our setup, we performed additional experiments with smaller spheres, of diameter 383 and 157 μm, using 10× and 15× magnification, respectively. The apparent horizontal displacements and the corresponding radial density gradient perturbations measured four diameters above a 383 μm sphere settling in a stratification with $N = 1.17$ s^{-1} are shown in Fig. 7. The signature of the wake can still clearly be detected by Synthetic Schlieren, although it is noticeably weaker, with apparent displacements that are about one quarter of those for the 780 μm sphere. After processing, the resulting radial density gradient perturbations are smaller by roughly the same ratio.

On an even smaller scale, cross-sectional data of the maximum detected horizontal displacement anywhere along the wake of a 157 μm sphere is presented in Fig. 8. While there is evidence of antisymmetric apparent displacements (highlighted by the dashed line that guides the eye) similar to those in Figs. 5 and 7, the magnitude of this signal is significantly smaller than for the larger spheres. Furthermore, the signal is compromised by the experimental noise, indicating that a 157 μm sphere lies at the lower detection bound for our experimental setup.

To quantify the background noise we performed experiments in the absence of a settling sphere. A

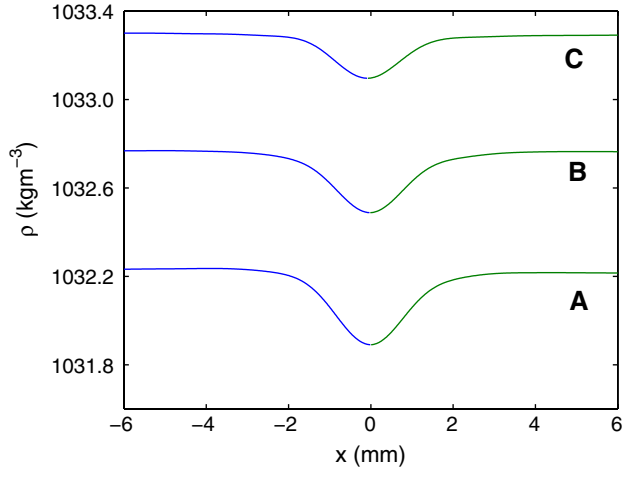

Fig. 6 Density perturbations in the wake of a 780 μm sphere, for transects A, B, and C in Fig. 4

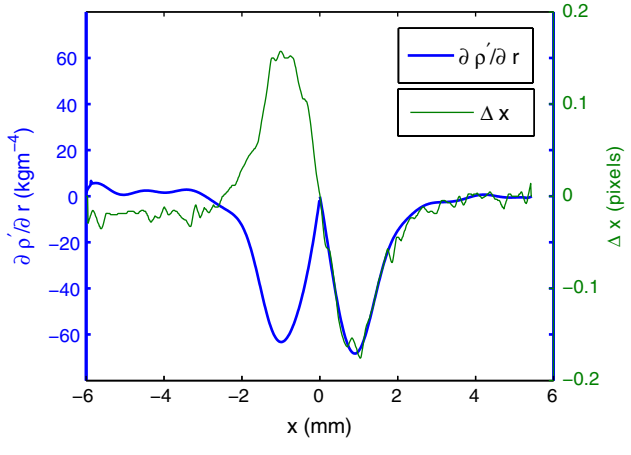

Fig. 7 Apparent horizontal displacements of the mask (*thin line*) and radial density gradient perturbation (*thick line*) for a 383 μm sphere

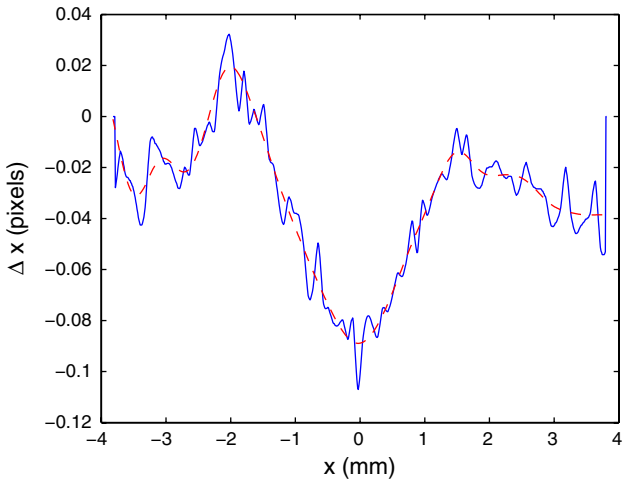

Fig. 8 Apparent horizontal displacements of the mask for a 157 μm sphere

stratification was established and left to stand for six hours, after which apparent displacements of the mask were determined using the same technique as above. The noise, likely due to a combination of small-scale mechanical vibrations, light intensity fluctuations and thermal disturbances both external and internal to the microscope, was on the order of 0.02 pixels. This is at the limit of what can be detected using pattern-matching techniques (Dalziel et al. 2000).

At the other end of the scale, for strong density gradient distortions the Synthetic Schlieren technique, which assumes small deflections of light rays, breaks down and is only capable of providing qualitative data. For a given sphere density, this effectively imposes an upper bound on the largest sphere whose wake can be studied quantitatively. Our experiments with a polystyrene sphere of 3.16 mm diameter, for example, produced mixing, which in turn generated highly nonlinear distortions of the mask.

5 Conclusion

In order to facilitate quantitative studies of environmental processes in the ocean involving the motion of microscale particles and organisms through stratified fluids, we have extended the application of Synthetic Schlieren techniques to the microscale. We tested our method on settling spheres, for which it is the structure of the wake rather than radiated internal waves that is primarily responsible for distorting the background stratification. In the wake, density gradient perturbations in the horizontal far exceed those in the vertical, requiring modification of the previous formulation of axisymmetric Synthetic Schlieren (Onu et al. 2003). For quantitative data, the method is limited to axisymmetric disturbances, while it can still provide qualitative information on the flow structure for non-axisymmetric disturbances or in the presence of strong mixing.

We could clearly detect and characterize the wake of 780 and 383 μm spheres, finding that lighter fluid is dragged downwards in a wake, the size of which greatly exceeds that of the sphere. As the sphere size was decreased further, the signal generated by the density gradient perturbations approached the background noise level. Even for a 157 μm sphere, however, we were able to detect a wake signature. We are currently working on applying this technique to elucidate the fluid mechanics of a stratified wake, in particular the suggested strong increase in drag coefficient (Torres et al. 2000).

Acknowledgments We wish to thank Bruce Sutherland for helpful discussions and for providing us with a version of the axisymmetric code for validation; Stuart Dalziel for thorough discourse on Synthetic Schlieren, as well as licences and support for Digiflow; Heidi Nepf for useful comments on the wake structure; Tanvir Ahmed for help in generating the mask.

References

Azam F, Long RA (2001) Sea snow microcosms. Nature 414:495–498

Burton RA (1949) A modified schlieren apparatus for large areas of field. J Opt Soc Am 39:907–909

Dalziel SB, Hughes GO, Sutherland BR (2000) Whole-field density measurements by 'synthetic schlieren'. Exp Fluids 28:322–335

Digiflow (2006) http://www.damtp.cam.ac.uk/lab/digiflow/

Flynn MR, Onu KO, Sutherland BR (2003) Internal wave excitation by a vertically oscillating sphere. J Fluid Mech 494:65–93

McIntyre S, Alldredge AL, Gotschalk CC (1995) Accumulation of marine snow at density discontinuities in the water column. Limnol Oceanogr 40:449–468

Onu K, Flynn MR, Sutherland BR (2003) Schlieren measurement of axisymmetric internal waves. Exp Fluids 35:24-31

Oster G (1965) Density gradients. Sci Am 213:70

Peacock T, Tabaei A (2005) Visualization of nonlinear effects in reflecting internal wave beams. Phys Fluids 17:061702

Richard H, Raffel M (2001) Principle and applications of the background oriented schlieren (BOS) method. Meas Sci Tech 12:1576–1585

Srdić-Mitrović AN, Mohamed NA, Fernando JS (1999) Gravitational settling of particles through density interfaces. J Fluid Mech 381:175–198

Sutherland RR, Dalziel SB, Hughes GO, Linden PF (1999) Visualisation and measurement of internal waves by 'synthetic schlieren'. Part I: vertically oscillating cylinder. J Fluid Mech 390:93–126

Toepler A (1864) Beobachtungen nach einer neuen optischen Methode. Max Cohen u. Sohn, Bonn

Torres CR, Hanazaki H, Ochoa J, Castillo J, Van Woert M (2000) Flow past a sphere moving vertically in a stratified diffusive fluid. J Fluid Mech 417:211–236

Venkatakrishnan L, Meier GEAL (2004) Density measurements using the Background Oriented Schlieren technique. Exp Fluids 37:237-247

Weyl FJ (1954) Analysis of optical methods. In: Ladenburg RW (eds) Physical measurements in gas dynamics and combustion. Princeton University Press, Princeton, pp. 3–25